Available online at www.sciencedirect.com
ScienceDirect
Ocean Modelling 19 (2007) 53–69
Ocean Modelling
www.elsevier.com/locate/ocemod

# The use of Argo for validation and tuning of mixed layer models

D.M. Acreman [a,*], C.D. Jeffery [b]

[a] Met Office, FitzRoy Road, Exeter EX1 3PB, UK
[b] National Oceanography Centre, Southampton, UK

Received 4 January 2007; received in revised form 18 June 2007; accepted 18 June 2007
Available online 30 June 2007

**Abstract**

We present results from validation and tuning of 1-D ocean mixed layer models using data from Argo floats and data from Ocean Weather Station Papa (145°W, 50°N). Model tests at Ocean Weather Station Papa showed that a bulk model could perform well provided it was tuned correctly. The Large et al. [Large, W.G., McWilliams, J.C., Doney, S.C., 1994. Oceanic vertical mixing: a review and a model with a nonlocal boundary layer parameterisation. Rev. Geophys. 32 (Novermber), 363–403] K-profile parameterisation (KPP) model also gave a good representation of mixed layer depth provided the vertical resolution was sufficiently high. Model tests using data from a single Argo float indicated a tendency for the KPP model to deepen insufficiently over an annual cycle, whereas the tuned bulk model and general ocean turbulence model (GOTM) gave a better representation of mixed layer depth. The bulk model was then tuned using data from a sample of Argo floats and a set of optimum parameters was found; these optimum parameters were consistent with the tuning at OWS Papa.


## 1. Introduction

The representation of the upper ocean boundary layer is an important component of ocean forecasting and climate models. Upper ocean boundary layer parameterisations must reproduce observed behaviour and careful setting of the tunable parameters is an important part of achieving this aim. Tuning and validation studies are often performed using 1-D models, which are computationally cheap to run but neglect advection. The meteorological and oceanographic observations taken at Ocean Weather Station Papa (OWS Papa) have been used to test model performance over an annual cycle in many previous studies (e.g. Martin, 1985; Gaspar et al., 1990; Large et al., 1994; Kantha and Clayson, 1994) as the effects of advection are thought to be small at this location.

More recently data from the Argo project have become available. Argo floats are autonomous profiling floats which measure temperature and salinity profiles with a typical period of ten days and have a working

* Corresponding author. Tel.: +44 (0) 1392 886083; fax: +44 (0) 1392 885681.
*E-mail address:* david.acreman@metoffice.gov.uk (D.M. Acreman).

1463-5003/$ - see front matter 
doi:10.1016/j.ocemod.2007.06.005

life of several years. These data allow validation of mixed layer models over an annual cycle with unprecedented spatial coverage.

This paper presents results from model validation and tuning using both the OWS Papa data and newer Argo data. Section 2 describes the three models used in this study and the solar radiation parameterisation common to all the models. Comparisons of the models to OWS Papa data and Argo data are presented in Section 3. Section 4 presents results from tuning the Kraus–Turner model, using OWS Papa data and data from a sample of Argo floats. The performance and sensitivities of the tuned model are investigated in Section 5. Conclusions are presented in Section 6.

## 2. Model descriptions

Three different upper ocean boundary layer models will be used in the subsequent studies. The first is based on the bulk model of Kraus and Turner (1967), the second is the two equation k-epsilon turbulence closure model from GOTM and the third is the K-profile parameterisation (KPP) model of Large et al. (1994). All three models assume horizontal homogeneity hence the effects of advection are not considered. The models are forced with prescribed fluxes and there is no relaxation to or assimilation of observed temperature and salinity profiles unless otherwise stated. Descriptions of the three model implementations and the solar radiation parameterisation, common to all three models, are presented below.

### *2.1. Kraus–Turner model*

The Kraus–Turner model uses an integrated form of the turbulent kinetic energy (TKE) equation to balance the generation of turbulence by wind mixing and convection with the work done in overturning stable stratification. In reality current shear also produces TKE but the Kraus–Turner model used here does not explicitly include a shear production term, unlike some bulk models.

From dimensional arguments the wind mixing energy $W$ can be represented by

$$W = \lambda \rho_{\mathrm{w}} u_*^3 \tag{1}$$

where $\rho_{\mathrm{w}}$ is the density of sea water, $u_*$ is the friction velocity and $\lambda$ is a non-dimensional, tunable parameter of order unity. The wind mixing energy is the rate at which the wind inputs turbulent kinetic energy into the ocean and has units of W m$^{-2}$. If the water column is unstable potential energy is released by convective overturning and a fraction of 0.15 of the potential energy is converted to TKE. The TKE is assumed to decay exponentially with depth with an e-folding length $\delta$. The partial mixing scheme of Thomson (1976) is used to balance wind mixing against work done in cases where an entire model level cannot be entrained into the mixed layer.

In contrast, momentum is not observed to be well mixed throughout the layer of uniform density near the surface so applying the Kraus–Turner model to momentum would not give realistic vertical profiles. Instead momentum is mixed using a simplified version of the KPP scheme which assumes neutral stability in the mixed layer (Gordon et al., 2000). A damping term is included in the velocity calculation, to prevent artificial velocity build up (Mellor, 2001) with a damping coefficient of (4 days)$^{-1}$ (Pollard and Millard, 1970).

The overall scheme for the vertical mixing of momentum and tracers is very similar to that used in the HadCM3 climate model (Gordon et al., 2000), but includes modifications used in the later HadGEM1 climate model (Johns et al., 2006).

### *2.2. GOTM configuration*

The General Ocean Turbulence Model (GOTM) is an open source, one-dimensional water column model for computing the solutions to the 1-D versions of the transport equations of momentum, heat and salt. It incorporates a number of different parameterisations for vertical turbulent mixing; for this study, we have chosen to use a two-equation k-epsilon turbulence closure scheme (Rodi, 1987), with dynamic dissipation rate equations for the length-scales.

Two-equation turbulence models use one transport equation for turbulent kinetic energy and another for a length scale-related quantity. These have proven to be a good compromise between complexity and simplification (Mellor and Yamada, 1974; Rodi, 1987; Canuto et al., 2001; Stips et al., 2002).

The equations for turbulent kinetic energy $k$ and its rate of dissipation $\epsilon$ are required for calculating the vertical eddy viscosity and diffusivity. The equations for $k$ and $\epsilon$ result from carrying out Reynolds decomposition, on the Navier–Stokes equations, into a mean flow and a fluctuating component. Since these equations are no longer closed, closure assumptions are required.

As described by Burchard et al. (1999) the transport equation for $k$ can be written as;

$$\frac{\partial k}{\partial t} - \frac{\partial}{\partial z}\left(\frac{v_t}{\sigma_k}\frac{\partial k}{\partial z}\right) = P + G - \epsilon \tag{2}$$

where $P$ is the production of $k$ by mean shear, $G$ is the production of $k$ by buoyancy and $\epsilon$ is the rate of dissipation of $k$.

$$P = v_t\left[\left(\frac{\partial u^2}{\partial z} + \frac{\partial v^2}{\partial z}\right)\right] \tag{3}$$

$$G = -\frac{v_t}{\sigma_t}N^2 \tag{4}$$

where $v_t$ is the turbulent friction coefficient, $u$ and $v$ are the components of velocity and $N$ is the Brunt–Vaisala frequency.

For horizontally homogeneous flows, the sum of the viscous and turbulent transport terms $D$ can be expressed by a simple gradient formulation

$$D_\epsilon = \frac{\partial}{\partial z}\left(\frac{v_t}{\sigma_\epsilon}\frac{\partial \epsilon}{\partial z}\right) \tag{5}$$

where $\sigma_\epsilon$ is the constant Schmidt number for $\epsilon$. The rate of dissipation $\epsilon$ is balanced according to

$$\frac{\partial \epsilon}{\partial t} = D_\epsilon + \frac{\epsilon}{k}(c_{\epsilon 1}P + c_{\epsilon 3}G + c_{\epsilon 2}\epsilon) \tag{6}$$

The dissipation rate can either be obtained directly from its parameterized transport equation or from any other model yielding an appropriate dissipative length scale, $l$. Then $\epsilon$ becomes

$$\epsilon = (c_\mu^0)^3\frac{k^{3/2}}{l} \tag{7}$$

This turbulence closure model is fitted to the logarithmic law of the wall. However, this law is not valid directly below the surface when wave breaking is present. The wave-enhanced layer is represented within GOTM by the wave breaking parameterisation suggested by Burchard (2001), using the empirical constant $cw = 100$ suggested by Craig and Banner (1994). We use the stability method as laid out by Kantha and Clayson (1994), and internal waves are incorporated within the model following Large et al. (1994).

The empirical constants used in the turbulence model are summarized in Table 1; we use the default GOTM v3.2 empirical coefficients for the $k$–$\epsilon$ model. The turbulent Schmidt number for $k$, $\sigma_k$, is a rough estimate (Rodi, 1987), the turbulent Schmidt number for the dissipation rate, $\sigma_\epsilon$, results from the law of the wall; $c_{\epsilon 1}$ and $c_{\epsilon 2}$ result from laboratory experiments with homogeneous shear flow and grid turbulence, respectively. For stable stratification ($N > 0$) $c_{\epsilon 3}$ results from fitting the steady state Richardson number to idealized experiments (see Burchard and Baumert 1995; Burchard and Bolding 2001), for unstable stratification ($N < 0$) $c_{\epsilon 3}$

Table 1
GOTM constants for the $k$–$\epsilon$ turbulence closure model according to Rodi (1987)

| $c_\mu^0$ | $\sigma_k$ | $\sigma_\epsilon$ | $c_{\epsilon 1}$ | $c_{\epsilon 2}$ | $c_{\epsilon 3}$, $N^2 > 0$ | $c_{\epsilon 3}$, $N^2 < 0$ |
|---|---|---|---|---|---|---|
| 0.5577 | 1.0 | 1.3 | 1.44 | 1.92 | 0.0 | 1.0 |

needs to be positive to retain a source of dissipation for free convection. The model time-step was set to 5 s with a uniform vertical model resolution of 10, 5, 2 or 0.5 m as specified.

### 2.3. The K-profile parameterisation scheme

The KPP scheme of Large et al. (1994) represents the turbulent mixing of a property $X$ using a diffusion equation which includes non-local transport effects

$$\frac{\partial X}{\partial t} = \frac{\partial}{\partial z}\left(K(z)\frac{\partial X}{\partial z} - \gamma\right) \tag{8}$$

where $K(z)$ is a depth dependent diffusion coefficient and $\gamma$ is a counter-gradient term which accounts for non-local effects. In the KPP scheme the diffusion coefficient in the boundary layer is parameterised by

$$K(z) = hw(\sigma)G(\sigma) \tag{9}$$

where $h$ is the depth of the boundary layer, $\sigma = d/h$ (where $d$ is the positive depth), $w(\sigma)$ is the turbulent velocity scale and $G(\sigma)$ is a shape function.

The shape function is assumed to be a polynomial of the form

$$G(\sigma) = a_0 + a_1\sigma + a_2\sigma^2 + a_3\sigma^3 \tag{10}$$

where $a_0$, $a_1$, $a_2$, $a_3$ are determined by applying the boundary conditions that $K = 0$ at $\sigma = 0$ (i.e. no turbulent flux at the surface) and that $K(z)$ and the vertical gradient of $K(z)$ match the background values at the base of the boundary layer. In this study the background mixing is determined using the method of Gordon et al. (2000).

The turbulent velocity scale $w(\sigma)$ is given by

$$w(\sigma) = \frac{\kappa u_*}{\phi(d/L)} \tag{11}$$

where $\kappa$ is the Von–Karman parameter, $u_*$ is the friction velocity and $\phi(d/L)$ is a depth dependent, empirically determined stability function which is a function of depth $d$ and the Obukhov length $L$. The function $\phi(d/L)$ is equal to unity under neutral forcing, hence $w(\sigma) = \kappa u_*$. The effect of $\phi(d/L)$ is to increase $w(\sigma)$ if the forcing is unstable and decrease $w(\sigma)$ if the forcing is stable. For more details of the stability functions see Large et al. (1994).

The boundary layer depth is the depth where the bulk Richardson number exceeds the threshold $Ri_c = 0.3$. The bulk Richardson number $Ri_b$ is given by

$$Ri_b = \frac{(B_r - B(d))d}{|\mathbf{V}_r - \mathbf{V}(d)|^2 + V_t^2(d)} \tag{12}$$

where $B_r$ is the buoyancy in the surface layer (averaged over $0.1h$), $B(d)$ is the buoyancy at depth $d$, $\mathbf{V}(d)$ is the vector difference of the velocity at depth $d$ and the average velocity in the surface layer, and $V_t$ is a term which accounts for shear due to turbulent velocity. The $V_t$ term is given by

$$V_t(d) = \frac{1.33}{Ri_c}N(d)wd \tag{13}$$

where $N(d)$ is the buoyancy frequency at depth $d$. The factor of 1.33 has been determined using the best fit parameters of Large et al. (1994). Some additional constraints are applied to the boundary layer depth. If the forcing is stable the boundary layer depth must be less than the Obukhov depth; the boundary layer depth is not allowed to exceed 80 m; and the boundary layer depth must not exceed the Ekman depth $h_E$ where

$$h_E = \frac{0.7u_*}{f} \tag{14}$$

and $f$ is the Coriolis parameter.

The counter-gradient term is non-zero only for tracers and only in the case of unstable forcing. The term is given by

$$\gamma = \frac{7.5\overline{wx_0}}{w(\sigma)h} \tag{15}$$

where $\overline{wx_0}$ is the flux of quantity $X$ at the surface, $w(\sigma)$ is the turbulent velocity scale and $h$ is the boundary layer depth.

### 2.4. Solar radiation

The absorption of solar radiation is treated identically in all models, using the double exponential representation of Paulson and Simpson (1977). The flux at depth $z$ is given by

$$S(z) = S(0)\{R\exp(z/\eta_1) + (1-R)\exp(z/\eta_2)\} \tag{16}$$

where $S(z)$ is the flux at depth $z$ and $z$ is measured negative downwards from zero at the ocean surface. The model partitions the solar flux into two components in the ratio $R$:$(1-R)$. The first component decays exponentially with depth with a length scale $\eta_1$ and the second component decays exponentially with depth with a length scale $\eta_2$. The parameters $\eta_1$, $\eta_2$ and $R$ depend on the optical clarity of the water. Paulson and Simpson (1977) give values of $\eta_1$, $\eta_2$ and $R$ for different Jerlov water types (Jerlov, 1976). The following experiments use either Jerlov water type IB ($\eta_1 = 1$ m, $\eta_2 = 17$ m and $R = 0.67$) or Jerlov water type II ($\eta_1 = 1.5$ m, $\eta_2 = 14$ m and $R = 0.77$). Unless otherwise stated the water type is assumed to be Jerlov IB (the same water type used in the UK Met Office ocean models) which is broadly representative of open ocean areas (Simonot and Le Treut, 1986).

## 3. Model comparisons

### 3.1. Model comparisons at OWS Papa

The Kraus–Turner model, KPP model and GOTM were run for 1 year starting on 1 March 1961, the same period used by Large et al. (1994). Model temperature and salinity profiles were initialised from observations and forcing was calculated from observed meteorological variables using bulk formulae. Wind stress, sensible heat flux and latent heat flux were calculated using version 3.0 of the COARE algorithm (Fairall et al., 2003). The down-welling longwave radiation was calculated using the formula of Josey et al. (2003) and the shortwave flux was calculated using the okta model of Dobson and Smith (1988) with albedo from Payne (1972). A freshwater flux was calculated using evaporation from the bulk formulae and precipitation taken from the SOC climatology (Josey et al., 1998) interpolated to the model time. The daily averages of the forcing fluxes are plotted in Fig. 1.

The net heat input from the fluxes described above is 42 W m$^{-2}$ for the 1 year period starting on 1 March 1961. This is not a closed cycle but previous studies have also found a net annual heat input at OWS Papa; a summary of heat fluxes at OWS Papa is given in Table 1 of Large (1996). A climatological average of $25 \pm 15$ W m$^{-2}$ was found by Large (1996) for the period 1960–1981 and an average of $32 \pm 19$ W m$^{-2}$ was found by Smith and Dobson (1984) for the period 1959–1975. The value of 42 W m$^{-2}$ found here is close to the upper error bound of these climatological averages but referring to Fig. 1b of Large (1996) shows that the period under consideration here was a time of higher than average net heat input. Comparing the net heat input of 42 W m$^{-2}$ found here with time series in Fig. 1b of Large (1996) shows good agreement.

Model vertical resolutions of 10 m, 5 m, 2 m and 0.5 m were used with sufficient vertical levels to give a total depth of 200 m. Plots of sea surface temperature (SST) and mixed layer depth for the four different resolutions used are shown in Figs. 2 and 3, respectively. Thin solid lines are from the Kraus–Turner model, dashed lines are from GOTM, dotted lines are from the KPP model and thick solid lines are from observations. The Kraus–Turner model uses parameter settings of $\lambda = 0.7$, $\delta = 100$ m which are the values currently used in the UK Met Office FOAM system (Bell et al., 2004) and the HadCM3 climate model (Gordon et al., 2000). The SST observations have been smoothed using a top-hat filter of width two days to average over tidal and inertial periods (similar to the treatment in Large et al. (1994) Section 5). The mixed layer depth is defined

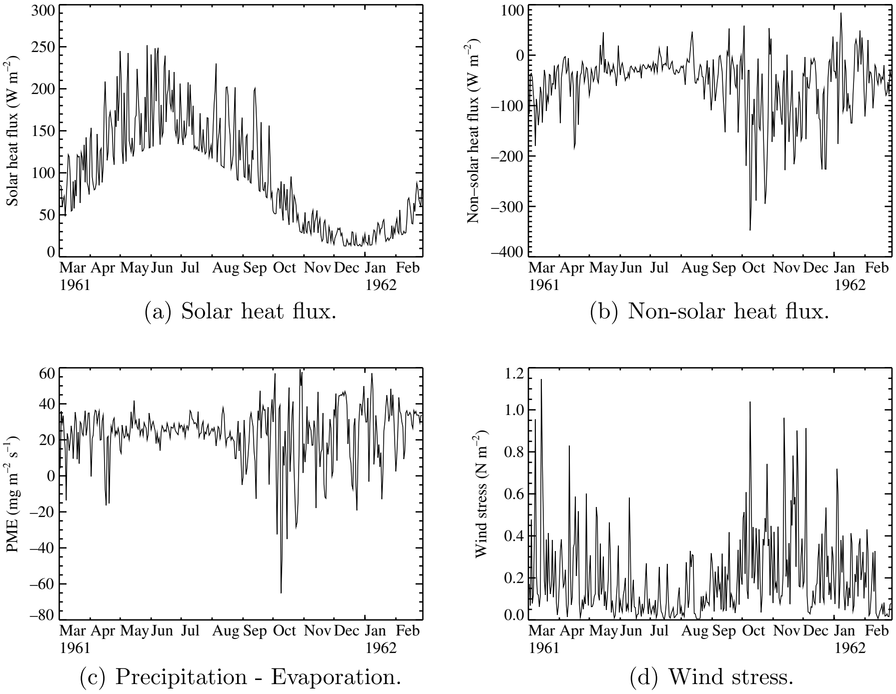


(a) Solar heat flux.

(b) Non-solar heat flux.

(c) Precipitation - Evaporation.

(d) Wind stress.

Fig. 1. Daily average forcing fluxes used in the OWS Papa experiment: (a) solar heat flux, (b) non-solar heat flux, (c) precipitation–evaporation and (d) wind stress.

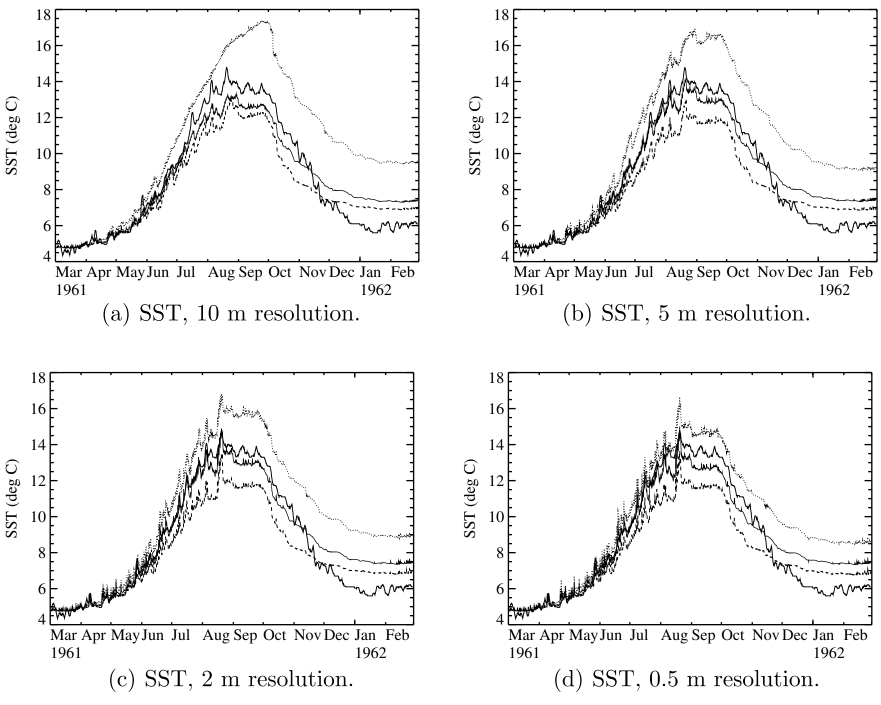


(a) SST, 10 m resolution.

(b) SST, 5 m resolution.

(c) SST, 2 m resolution.

(d) SST, 0.5 m resolution.

Fig. 2. One year evolution of sea surface temperature at OWS Papa for model runs with 10 m, 5 m, 2 m and 0.5 m resolution. Thin solid lines are from the Kraus–Turner model, dashed lines are from GOTM, dotted lines are from the KPP model and thick solid lines are from observations: (a) SST, 10 m resolution; (b) SST, 5 m resolution; (c) SST, 2 m resolution and (d) SST, 0.5 m resolution.

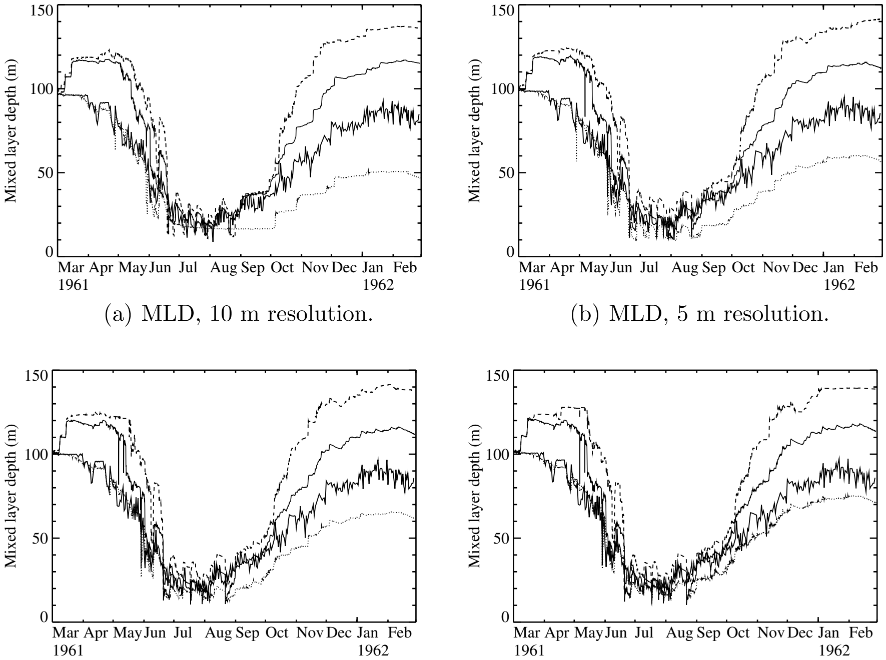


(a) MLD, 10 m resolution.
(b) MLD, 5 m resolution.
(c) MLD, 2 m resolution.
(d) MLD, 0.5 m resolution.

Fig. 3. One year evolution of mixed layer depth at OWS Papa for model runs with 10 m, 5 m, 2 m and 0.5 m resolution. Thin solid lines are from the Kraus–Turner model, dashed lines are from GOTM, dotted lines are from the KPP model and thick solid lines are from observations: (a) MLD, 10 m resolution; (b) MLD, 5 m resolution; (c) MLD, 2 m resolution and (d) MLD, 0.5 m resolution.

according to the "optimal mixed layer depth" of Kara et al. (2000), i.e. the depth at which the potential density has increased by an amount corresponding to temperature difference of 0.8 °C at the surface.

The Kraus–Turner model produces mixed layers which are too deep, except for the summer months when the model performs well. The model mixed layer depth is not strongly dependent on vertical resolution and it is apparent that, at all resolutions, the Kraus–Turner model needs to be re-tuned if it is to perform acceptably at OWS Papa. The Kraus–Turner SSTs are somewhat colder than the observed SSTs, consistent with too much vertical mixing. The model summer-time SST shows a resolution dependence; higher resolution runs have more realistic SSTs and more realistic SST variability than the lower resolution runs. As vertical resolution increases, the thermal inertia of the top model level is reduced which allows a more rapid response to changes in the heat input. This effect is most noticeable in summer when the mixed layer is shallow and the heat input is not mixed downwards away from the surface layers. The observed SST is seen to depart significantly from all models in the latter part of the year. Large (1996) compares surface heat fluxes at OWS Papa, calculated using bulk formulae, with the heat flux inferred from changes in heat content and concludes that heat fluxes and storage are balanced for much of the year (until August) but that there are significant differences between August and December. Referring to Fig. 3 of Large (1996) shows that the discrepancy is particularly large in November and December, the same months in which the model SST departs most rapidly from the observed SST in Fig. 2. Consequently the large difference between model and observed SST after October may be attributed to a departure from 1 dimensional heat balance during November and December.

The mixed layer depth from GOTM is very similar to that from the Kraus–Turner model during the first half of the run and shows a similar over deepening at later times. Some differences are seen in GOTM runs at different resolutions but the mixed layer depths from all four runs are similar, even at the lowest vertical resolution. As the mixed layer depth from GOTM was observed to be too deep the Craig–Banner wave breaking term was switched off in these runs resulting in slightly shallower mixed layer depths.

The KPP scheme gives a good mixed layer depth representation during the first half of the year, even with a coarse vertical resolution. However the deepening phase is poorly represented at low resolution, particularly at the lowest vertical resolution of 10 m. The 10 m vertical resolution run exhibits step-like increases in the mixed layer depth between October and December. These step-like increases are also seen in the boundary layer depth diagnosed by the KPP scheme. The increases in the KPP boundary layer depth occur slightly before the increases in diagnosed mixed layer depth indicating that the former drives the latter. The mixing coefficients are proportional to the boundary layer depth so this is expected. At higher vertical resolutions the KPP model performance improves and at 0.5 m resolution the KPP model represents mixed layer depth significantly better than the other models. The resolution dependence of the KPP model was noted by Large et al. (1994) in sensitivity studies under idealised forcing (see Appendix C of Large et al., 1994). The SST from the KPP model also shows a lack of variability at low resolution and at the highest resolution the variability in all the model SSTs is similar.

### 3.2. Model comparisons using Argo float Q4900131

A case study was performed using data from Argo float Q4900131 over the period November 2002–October 2003, when the float was located close to the OWS Papa site. The Kraus–Turner model, KPP model and GOTM were run at 0.5 m vertical resolution with 500 vertical levels. Initial temperature and salinity profiles were obtained by interpolating observed profiles, from the Argo float, onto the model vertical levels. Forcing fluxes of heat, momentum and moisture were taken from the UK Met Office NWP system. The fluxes are generated 6 h and were interpolated to hourly values, plots of the daily averaged fluxes are shown in Fig. 4. The fluxes are generally similar to the fluxes used in the OWS Papa experiment (see Fig. 1) apart from the freshwater flux. The difference may be attributed to the greater variability in precipitation from the NWP model compared to using a precipitation climatology. Although the temporal variability of the freshwater flux is different in the two experiments the average freshwater input over the year is similar; for OWS Papa the average freshwater input is 23 mg m$^{-2}$ s$^{-1}$ and for this experiment is it 25 mg m$^{-2}$ s$^{-1}$. There is a net heat input from these fluxes of 25 W m$^{-2}$ which is smaller than the 42 W m$^{-2}$ heat input from the OWS Papa fluxes but in good agreement with the observations. As the solar flux from the UK Met Office NWP system is in a different

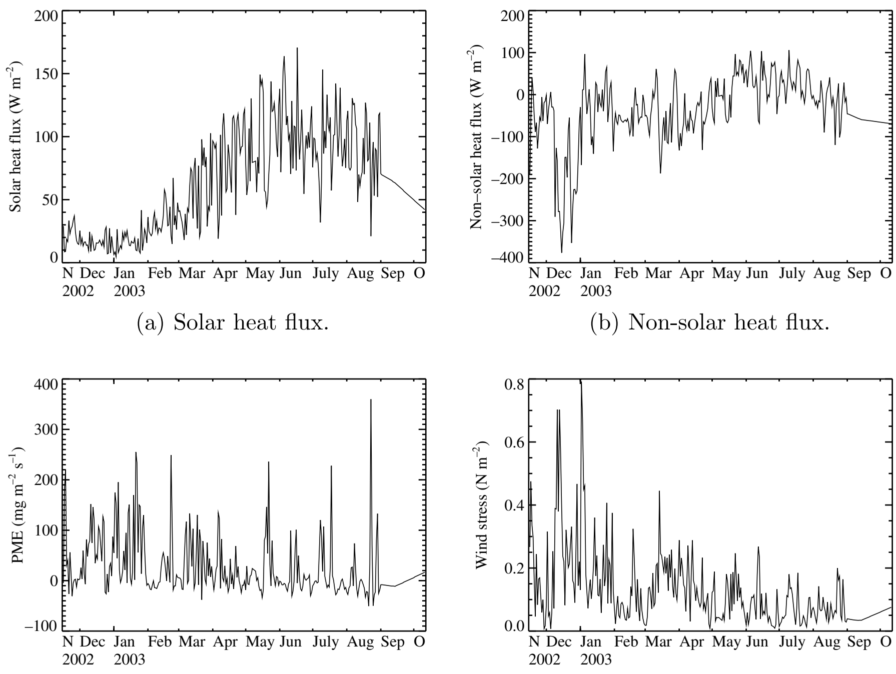


(a) Solar heat flux. (b) Non-solar heat flux.

(c) Precipitation - Evaporation. (d) Wind stress.

Fig. 4. Daily average forcing fluxes used with Argo float Q4900131: (a) solar heat flux, (b) non-solar heat flux, (c) precipitation–evaporation and (d) wind stress.

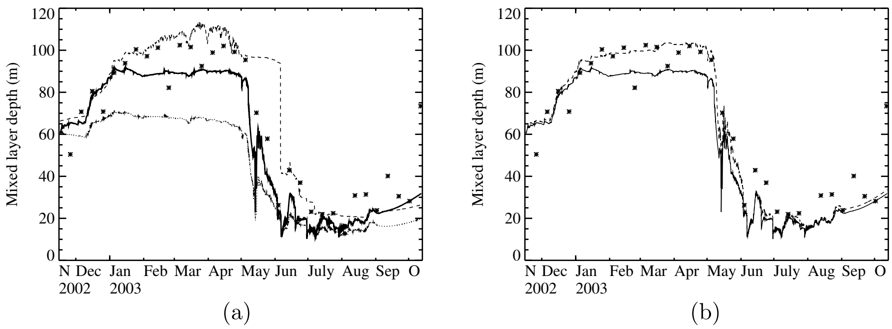


Fig. 5. (a) Mixed layer depth from the Kraus–Turner model (solid line), KPP model (dotted line) and GOTM (dashed line) models run at the location of float Q4900131. Mixed layer depths from the Argo float are plotted as points. The Kraus–Turner model uses $\lambda = 0.7$, $\delta = 100$ m. (b) The Kraus–Turner model with freshwater flux (solid line) and without freshwater flux (dashed line).

band to that used by Paulson and Simpson (1977) it was necessary to change the value of the $R$ parameter, described in Section 2.4, from 0.67 to 0.38 for Jerlov type IB water.

Mixed layer depths from the Kraus–Turner model, KPP model and GOTM (with the Craig–Banner term included) are shown in Fig. 5a, with the observed mixed layer depths from the Argo float plotted as points. The Kraus–Turner model uses parameter settings of $\lambda = 0.7$, $\delta = 100$ m as in the previous section. The mixed layer depth from the Kraus–Turner model (solid line) is initially good but becomes too shallow after January. The KPP scheme (dotted line) gives mixed layers which are too shallow compared to the observations and lack variability in summer. The GOTM mixed layer depth (dashed line) is the most realistic of all the models and best captures the deepening phase at the start of the run. The Kraus–Turner model and GOTM, which were too deep when validated at OWS Papa, perform well in this case.

In order to assess the impact of the freshwater flux, the Kraus–Turner model was run with zero freshwater flux. Results with the freshwater flux included (solid line) and with no freshwater flux (dashed line) are shown in Fig. 5b. With no freshwater flux the modelled mixed layer depth is significantly deeper from the beginning of January to the end of April. A net input of freshwater provides a positive buoyancy flux which tends to inhibit mixing, so when the freshwater input is removed the mixed layer tends to deepen more. The effect of freshwater flux on vertical mixing has also been studied by McCulloch et al. (2004). They found that freshwater flux affected mixed layer depth at a location in the North East Atlantic near 40°N in December. The Argo float used in this case study is at a similar latitude also in the Eastern part of the ocean basin (albeit in the Pacific) and also shows a significant influence of freshwater flux in winter.

## 4. Kraus–Turner model tuning

### *4.1. Kraus–Turner model tuning at OWS Papa*

The Kraus–Turner model did not compare well with observations at OWS Papa, other than in summer when the mixed layer was shallow. In contrast the KPP model performed well at OWS Papa, provided the vertical resolution was sufficiently high, indicating that the forcing fluxes are not significantly in error. The performance of the Kraus–Turner model might be improved by tuning the parameters $\lambda$ (generation of TKE) and $\delta$ (decay of TKE with depth) described in Section 2.1. The values of $\lambda = 0.7$ and $\delta = 100$ m used in HadCM3 (Gordon et al., 2000) were chosen to give the same dissipation as the MILE experiment (Davis et al., 1981). In contrast the KPP model was tuned at OWS Papa by (Large et al., 1994) so is expected to perform well at this location, although some differences are expected between the results presented here and those of Large et al. (1994) due to different treatments of forcing fluxes and absorption of solar radiation.

The Kraus–Turner model was run using different values of the $\lambda$ and $\delta$ parameters. The $\lambda$ parameter was varied from 0 to 1.5 in steps of 0.025 and $\delta$ was varied from 0 m to 150 m in steps of 10 m. For each model run the mean and RMS difference between the model and observed mixed layer depth was calculated each time an observation was available. These mean and RMS errors were then averaged to obtain average mean and

RMS mixed layer depth errors over the annual cycle. The tuning experiment was run three times with different vertical resolutions and Jerlov water types. The first run used a vertical resolution of 10 m and a Jerlov type IB water; this is typical of a UK Met Office ocean model used for either operational ocean forecasting or climate purposes. The second run used a vertical resolution of 10 m and a Jerlov type II water. Gaspar (1988) used Jerlov type II water in a 1-D mixed layer model at OWS Papa and Large et al. (1994) perform runs with type IA, type II and a time varying water type. The third run used a higher vertical resolution of 2 m and a Jerlov type IB water. Plots showing how the mean and RMS errors vary with different values of the $\lambda$ and $\delta$ parameters are shown in Fig. 6. A negative mean error indicates that the model is too deep compared to the observations.

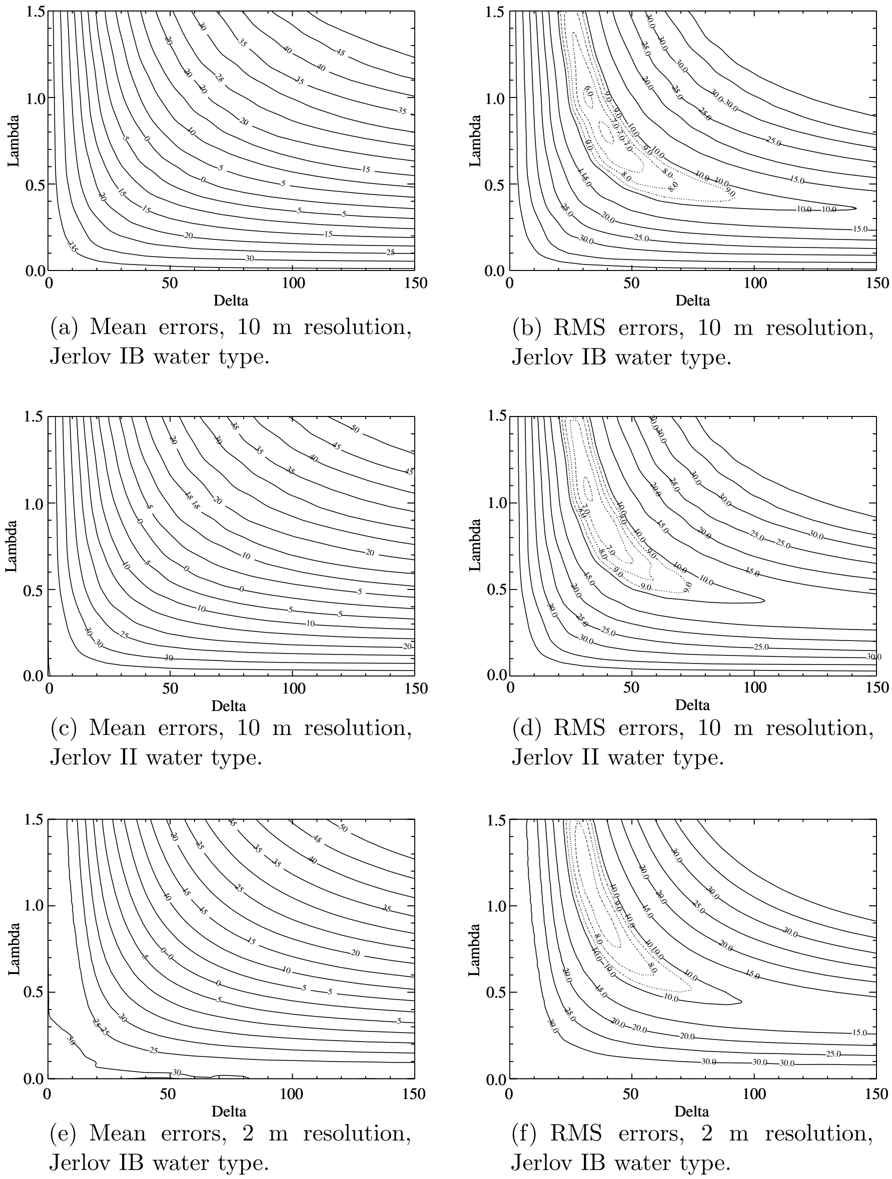


(a) Mean errors, 10 m resolution, Jerlov IB water type.

(b) RMS errors, 10 m resolution, Jerlov IB water type.

(c) Mean errors, 10 m resolution, Jerlov II water type.

(d) RMS errors, 10 m resolution, Jerlov II water type.

(e) Mean errors, 2 m resolution, Jerlov IB water type.

(f) RMS errors, 2 m resolution, Jerlov IB water type.

Fig. 6. Mean and RMS errors as a function of $\delta$ and $\lambda$ parameters from the OWS Papa tuning experiment. The tuning experiment was performed three times. Firstly at 10 m resolution with type IB water, secondly at 10 m resolution with type II water and thirdly at 2 m resolution with type IB water. Solid contours are at intervals of 5 m, dashed contours are at intervals of 1 m. (a) Mean errors, 10 m resolution, Jerlov IB water type, (b) RMS errors, 10 m resolution, Jerlov IB water type, (c) mean errors, 10 m resolution, Jerlov II water type, (d) RMS errors, 10 m resolution, Jerlov II water type, (e) mean errors, 2 m resolution, Jerlov IB water type and (f) RMS errors, 2 m resolution, Jerlov IB water type.

At 10 m resolution, with Jerlov type IB water, the minimum RMS errors are with $\lambda = 0.775$, $\delta = 40$ m which also gives mean errors close to zero. If $\delta$ is fixed at 100 m the best value of $\lambda$ is approximately 0.4, much lower than the value of 0.7 used in the previous section when $\delta$ was 100 m. When Jerlov type II water is assumed the minimum RMS errors are with $\lambda = 1.125$, $\delta = 30$ m. Although the optimum parameters are different, the overall distribution of RMS errors is very similar to the previous case. At 2 m resolution, with Jerlov water type IB, the smallest errors are with $\lambda = 1.275$, $\delta = 30$ m. The tuning experiment was also performed with Jerlov type IB water at 0.5 m resolution, giving optimum parameters of $\lambda = 1.225$, $\delta = 30$ m. The experiment was additionally performed using the uppermost 14 levels from the UK Met Office FOAM system (Bell et al., 2004). This comprises 14 vertical levels with level bases at 10.0 m, 20.0 m, 30.0 m, 40.2 m, 55.5 m, 78.5 m, 113.0 m, 164.8 m, 242.6 m, 359.4 m, 534.7 m, 797.9 m, 1193.2 m, 1808.5 m. Optimum parameters at the FOAM vertical resolution are $\lambda = 0.925$, $\delta = 40$ m. Changes in vertical resolution and Jerlov water type have an effect on the choice of optimum parameter settings however the overall distribution of errors does not vary greatly under these changes. The region bounded by the 10 m RMS error contour is similar in all cases and choosing parameters within this contour (e.g. $\lambda = 1.0$, $\delta = 30$ m) will give small RMS errors for all resolutions and both water types considered here.

There is a significant interaction between the $\lambda$ and $\delta$ parameters such that small RMS errors can also be obtained with larger $\lambda$ and smaller $\delta$ (greater generation of TKE but more rapid dissipation with depth) or smaller $\lambda$ and larger $\delta$ (less generation of TKE but less rapid dissipation with depth). These results show the importance of considering interactions between parameters when tuning this model. In order to gain a better understanding of the relationship between the $\lambda$ and $\delta$ parameters, the tuning experiment was repeated for shorter time periods. The first time period was 1 March–31 May, a time when the mixed layer is shoaling; the second period is 1 June to 30 September, when there is a shallow mixed layer; the third period is from 1 October to 31 December when the mixed layer deepens. Plots from tuning runs using 2 m vertical resolution are shown in Fig. 7. If the mixing energy at the surface is $\lambda\rho_w u_*^3$ and the available energy decays exponentially with depth then the mixing energy reaching the base of a well-mixed layer of depth $h$ is given by

$$\lambda\rho_{\mathrm{w}} u_*^3 \exp(-h/\delta) \tag{17}$$

If we require that some fixed amount of mixing energy $f\rho_{\mathrm{w}} u_*^3$ is available at the base of the well mixed layer, in order to produce a given deepening of the mixed layer, then $\lambda$ and $\delta$ must satisfy the relation

$$\lambda \exp(-h/\delta) = f \tag{18}$$

This relation is plotted in Fig. 7 (heavy dashed line) for different values of $f$. The well mixed layer depth $h$ is calculated as the average mixed layer depth from observations, using a temperature difference of 0.1 °C, over the time period in question. The depth calculated with this small temperature difference should be representative of the depth of active mixing. The average well mixed layer depths are 40 m (March–May), 20 m (June–September) and 41 m (October–December). The general shape of the contours, for all three time periods, is broadly consistent with the results from the year-long run, but some differences are apparent. In March–May there is a preference for a small value of $\delta$ and a large value of $\lambda$; the small value of $\delta$ prevents mixing energy from penetrating too deeply. In the October–December period there is not the same requirement for a small $\delta$ and a large $\lambda$, and small RMS errors can be obtained provided the relationship between $\lambda$ and $\delta$ is observed. In the October–December period the important factor is the mixing energy available at the base of the well mixed layer whereas in the March–May period there is a requirement that the mixing energy is not allowed to penetrate too deeply. In March–May and October–December the relationship between $\lambda$ and $\delta$ is well represented by $f = 0.2$–$0.4$, i.e. the mixing energy available at the depth of active mixing is (0.2–0.4) $\rho_{\mathrm{w}} u_*^3$. In June–September, when the mixed layer is shallower, the mixing energy available at the depth of active mixing is greater ((0.4–0.7) $\rho_{\mathrm{w}} u_*^3$).

### 4.2. Model tuning using Argo data

Operational forecasting systems will often require a lower vertical resolution than those used in the previous section, in order to strike a balance between model performance and the computational expense of running the model. This section investigates tuning of the Kraus–Turner model at a coarser vertical resolution,

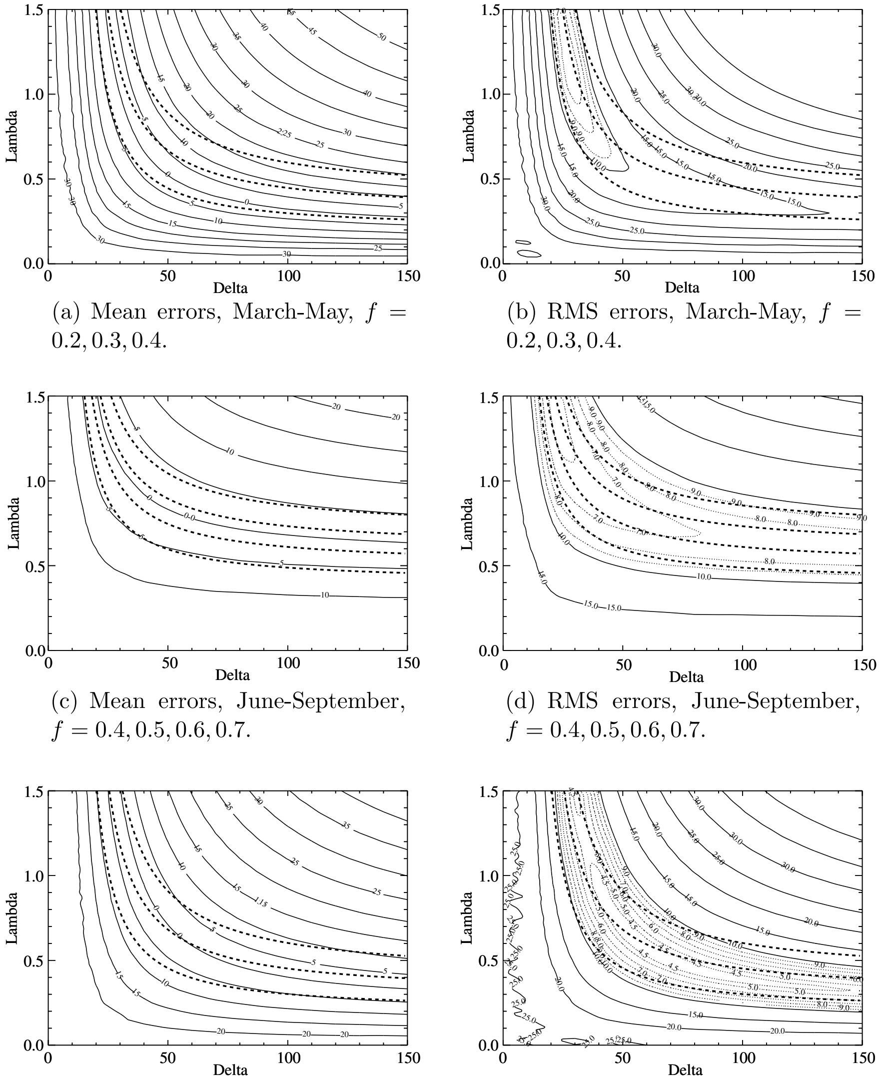


(a) Mean errors, March-May, $f = 0.2, 0.3, 0.4$.

(b) RMS errors, March-May, $f = 0.2, 0.3, 0.4$.

(c) Mean errors, June-September, $f = 0.4, 0.5, 0.6, 0.7$.

(d) RMS errors, June-September, $f = 0.4, 0.5, 0.6, 0.7$.

(e) Mean errors, October-December, $f = 0.2, 0.3, 0.4$.

(f) RMS errors, October-December, $f = 0.2, 0.3, 0.4$.

Fig. 7. Mean and RMS errors as a function of $\delta$ and $\lambda$ parameters from the OWS Papa tuning experiment. Tuning has been carried out during March–May, June–September and October–December. The heavy dashed line is the relationship between $\lambda$ and $\delta$ if the mixing energy at the base of the mixing layer is required to be constant. (a) Mean errors, March–May, $f = 0.2, 0.3, 0.4$, (b) RMS errors, March–May, $f = 0.2, 0.3, 0.4$, (c) mean errors, June–September, $f = 0.4, 0.5, 0.6, 0.7$, (d) RMS errors, June–September, $f = 0.4, 0.5, 0.6, 0.7$, (e) mean errors, October–December, $f = 0.2, 0.3, 0.4$ and (f) RMS errors, October–December, $f = 0.2, 0.3, 0.4$.

but using the wide geographical coverage offered by Argo data. The vertical levels were the uppermost 14 levels from the UK Met Office FOAM system, as described in Section 4.1.

Initial profiles of temperature and salinity were obtained by interpolating Levitus climatology onto the model levels. The models were then run for one year, starting in November 2002, using fluxes from the Met Office NWP system as described in Section 3.2.

When a float report was available a comparison was made between the model mixed layer depth and the observed mixed layer depth (calculated from the Argo temperature and salinity profiles) and mean and RMS difference was calculated. After the comparison was made the temperature and salinity profiles were assimilated into the model over a 10 day window using a linear weighting.

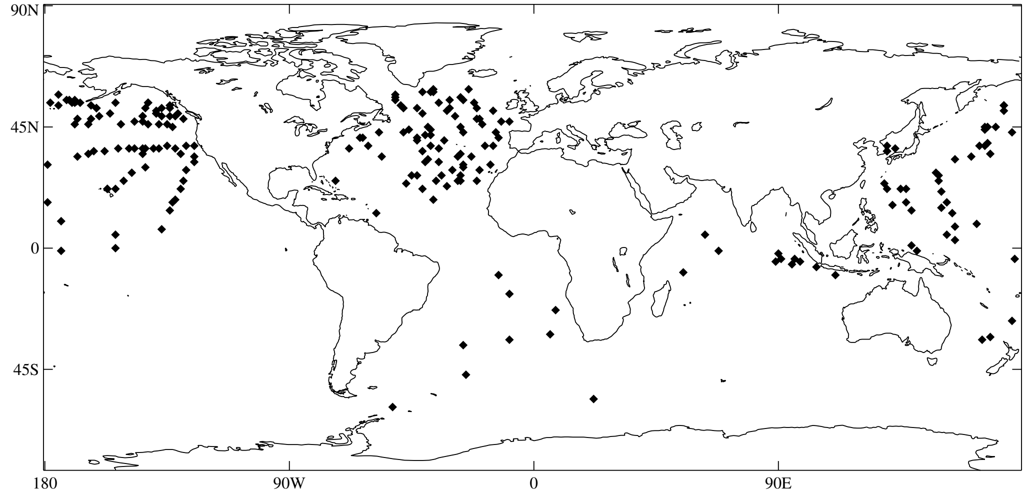


Fig. 8. Locations of the 218 Argo floats used in the tuning experiment.

A sample of Argo floats was selected by choosing floats with at least 30 reports, at approximately 10 day intervals, over the period November 2002–October 2003. This gave a sample of 218 floats whose locations are plotted in Fig. 8. The models were run for each of the floats in the sample with different values of the $\lambda$ and $\delta$

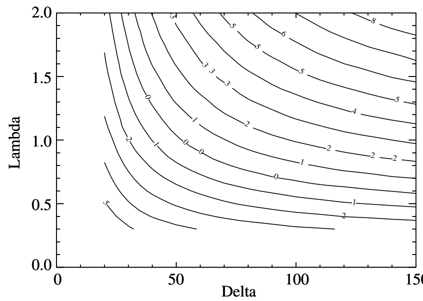


(a) Mean mixed layer depth error with assimilation of all profiles.

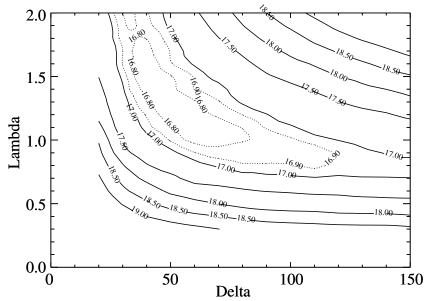


(b) RMS mixed layer depth error with assimilation of all profiles.

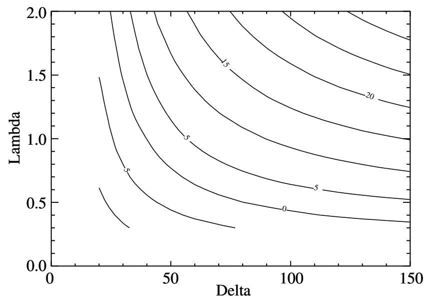


(c) Mean mixed layer depth error with assimilation of one profile only.

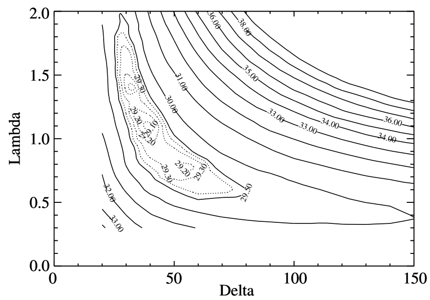


(d) RMS mixed layer depth error with assimilation of one profile only.

Fig. 9. Mean and RMS errors as a function of $\lambda$ and $\delta$ parameters from the Argo tuning experiment. The experiment was run twice; once with assimilation of all profiles (top) and secondly with assimilation of the first set of profiles only (bottom). (a) Mean mixed layer depth error with assimilation of all profiles, (b) RMS mixed layer depth error with assimilation of all profiles, (c) mean mixed layer depth error with assimilation of one profile only and (d) RMS mixed layer depth error with assimilation of one profile only.

parameters. Mean and RMS differences between model and observed mixed layer depths were calculated for each float report and averaged over all reports for all floats in the sample. The effects of horizontal advection were quantified by comparing the observed change in mixed layer heat content with the heat input from the forcing fluxes. If the observed change in mixed layer heat content differed by more than 50 W m$^{-2}$ from the heat input from the forcing fluxes the report was excluded from the calculation of average errors. 50 W m$^{-2}$ was estimated to be the combined error in heat flux and heat storage based on Fig. 3 of Large (1996). Plots of the mean and RMS errors, averaged over all floats, for different values of $\lambda$ and $\delta$, are plotted in Fig. 9a and b, respectively. The minimum RMS errors are with $\lambda = 1.5$, $\delta = 40$ m with a corresponding mean error of $-0.7$ m (a negative mean error indicates the model is too deep on average). These results are similar to the results from tuning the Kraus–Turner model to OWS Papa in that there is a requirement for a larger $\lambda$ and smaller $\delta$ than the values of $\lambda = 0.7$, $\delta = 10$ m used in HadCM3 and FOAM, however the best values of $\lambda$ and $\delta$ are larger than those from the OWS Papa experiment indicating greater generation of TKE and less rapid decay with depth. The inclusion of assimilation was found to increase the model temperature gradients so when assimilation is included it is expected that larger values of $\lambda$ and $\delta$ are required to reproduce the observed mixed layer deepening, due to the need to mixing against greater stratification.

In order to assess the impact of data assimilation on the choice of $\lambda$ and $\delta$ parameters the tuning experiment was repeated but only temperature and salinity profiles from the first float report were assimilated. The assimilation of profiles from only the first report ensures that the initial model profiles are realistic but prevents the assimilation from increasing the thermocline gradient during the course of the simulation. This is also a better comparison with the OWS Papa results, which did not include data assimilation. Mean and RMS errors are plotted in Fig. 9c and d, respectively. The distribution of RMS errors is now more similar to the results from tuning at OWS Papa than the previous case. The smallest RMS errors are with $\lambda = 1.1$, $\delta = 40$ m compared to values of $\lambda = 0.925$, $\delta = 40$ m for OWS Papa at the same vertical resolution. These results suggest that different parameter choices are required in models with data assimilation (e.g forecast models) than in models with no data assimilation (e.g. climate models).

## 5. Model sensitivities and performance of tuned Kraus–Turner scheme

### 5.1. OWS Papa

This section examines the performance of the tuned Kraus–Turner model and the sensitivity of the Kraus–Turner and KPP models to differences in water type and the assumed freshwater flux. The Kraus–Turner and KPP models were run at 2 m resolution with a Jerlov type IB water; the Kraus–Turner model used parameters of $\lambda = 1.275$, $\delta = 30$ m derived from the tuning in Section 4.1. Mixed layer depths and SSTs are plotted in Fig. 10a and b. The tuned Kraus–Turner model gives a good representation of mixed layer depth and the representation of SST is good until November, when it is thought that advective effects become important, as discussed in Section 3.1. At this resolution the KPP model tends to produce mixed layers which are too shallow and SSTs which are too warm, although it should be emphasised that the KPP model has not been tuned using the flux and water type parameterisations in use here. Large et al. (1994) use a more sophisticated time varying water type parameterisation than used here so a direct comparison between the KPP and Kraus–Turner will tend to favour the Kraus–Turner model.

The buoyancy input from a positive freshwater flux can cause significant changes to the mixed layer depth (McCulloch et al., 2004). In order to assess the significance of the freshwater flux the models were re-run with the freshwater flux set to zero. SST is plotted in Fig. 10c and mixed layer depth is plotted in Fig. 10d. The mixed layer depths from both models have been slightly altered with a slight improvement in the KPP mixed layer depth, however the summer-time SSTs from the Kraus–Turner model have become too cold. The freshwater flux does have some effect on the simulated annual cycles of mixed layer depth and SST but it does not appear to be a dominant process in this case.

Another set of model runs was performed with the freshwater flux reinstated but with the water type changed to Jerlov type II from Jerlov type IB. The Kraus–Turner model parameters were kept as $\lambda = 1.275$, $\delta = 30$ m. SST is plotted in Fig. 10e and mixed layer depth is plotted in Fig. 10f. The change of water type does not have a significant impact on the mixed layer depths but does have an impact on the SST. SSTs with

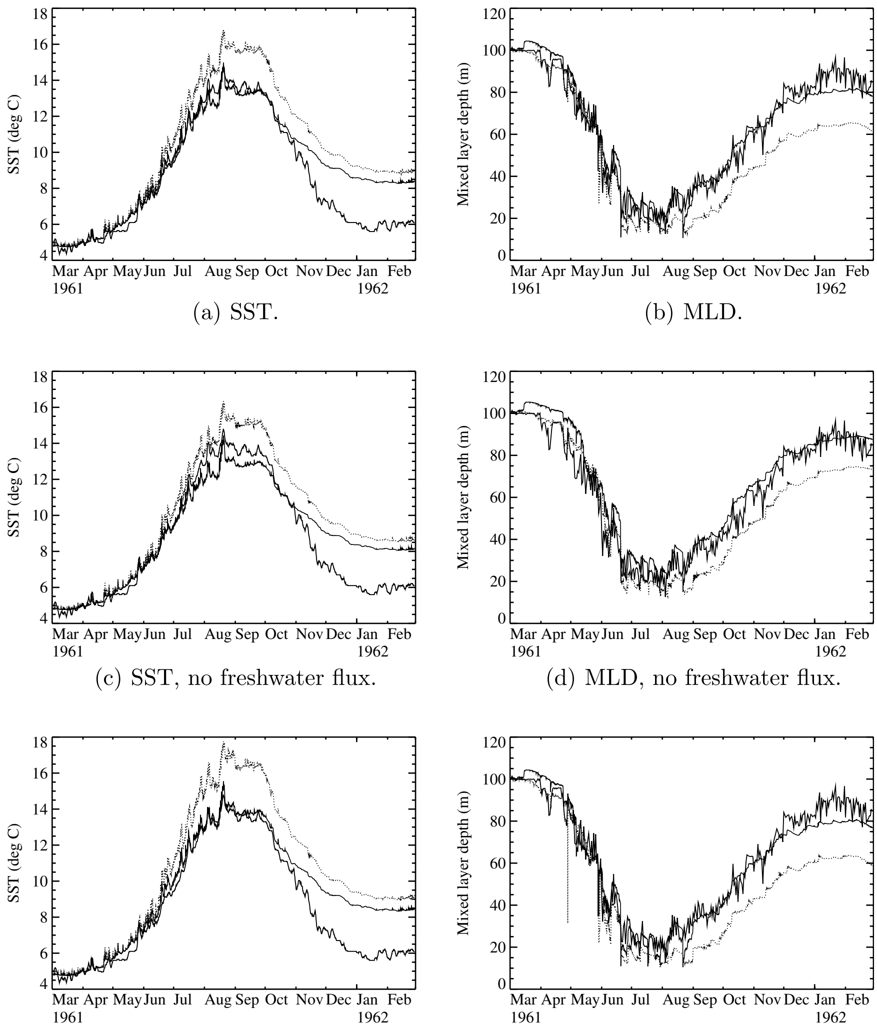


(a) SST. (b) MLD.

(c) SST, no freshwater flux. (d) MLD, no freshwater flux.

(e) SST, Jerlov type II. (f) MLD, Jerlov type II.

Fig. 10. One year evolution of sea surface temperature (left) and mixed layer depth (right). Thin solid lines are from the Kraus–Turner model, dotted lines are from the KPP model and thick solid lines are from observations: (a) SST; (b) MLD; (c) SST, no freshwater flux; (d) MLD, no freshwater flux; (e) SST, Jerlov type II and (f) MLD, Jerlov type II.

the type II water are warmer than with the type IB water, as expected if the water is more turbid and absorption of solar radiation is occurring closer to the surface. The Kraus–Turner model SSTs are warmer than before and agree slightly better with the observations. These results indicate that care should be taken when using SST to validate mixed layer models as the water type used by the model can affect the results. The KPP model exhibits a rapid shoaling of the mixed layer at the end of April. This is caused by a period of heating, which results in the brief formation of a shallow mixed layer, before the water column is then mixed by an input of wind mixing energy. When the more turbid type II water is used the solar radiation is absorbed nearer the surface, making the formation of shallow mixed layers more effective. The Kraus–Turner model does not exhibit the rapid shoaling of the mixed layer at the end of April as it performs more near surface mixing than the KPP model at this time.

### 5.2. Argo float Q4900131

The mixed layer depth from the Kraus–Turner model, with $\lambda = 1.1$, $\delta = 40$ m, is plotted in Fig. 11a with the mixed layer depths from GOTM and the KPP model. The performance of the Kraus–Turner scheme with

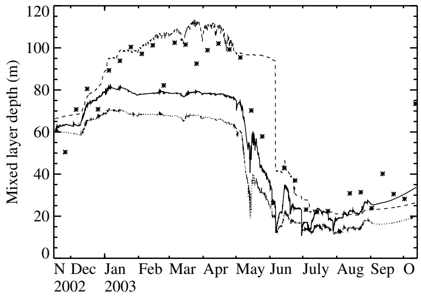


(a)

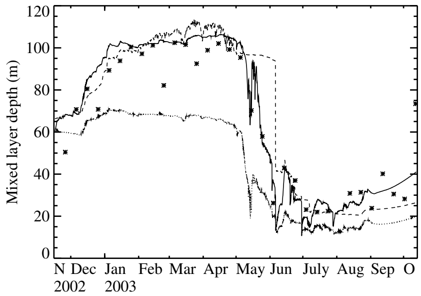


(b)

Fig. 11. Mixed layer depth from the Kraus–Turner model (solid line), KPP model (dotted line) and GOTM (dashed line) models run at the location of float Q4900131. Mixed layer depths from the Argo float are plotted as points. The Kraus–Turner model uses $\lambda = 1.1$, $\delta = 40$ m (left) and $\lambda = 1.1$, $\delta = 100$ m (right).

these parameters is similar to the performance of the untuned model although $\lambda = 1.1$, $\delta = 40$ m performs worse when the mixed layer is deep and better when the mixed layer is shallow, in particular the variability after May is improved.

If the Kraus–Turner parameters are changed to $\lambda = 1.1$, $\delta = 100$ m (shown in Fig. 11b) the annual cycle is well represented. Compared to the parameters of $\lambda = 1.1$, $\delta = 40$ m derived in Section 4.1 this particular case requires much less dissipation of TKE with depth (larger value of $\delta$) for the same TKE generation (same value of $\lambda$). This may indicate less rapid dissipation of TKE but care must be taken not to over interpret this result due to the degeneracy of the $\lambda$ and $\delta$ parameters.

## 6. Conclusions

The Kraus–Turner bulk model, the KPP scheme of Large et al. (1994), and the GOTM turbulence closure model were compared at OWS Papa and against data from an Argo float. The bulk model and GOTM were found to mix too deeply at OWS Papa but to give a good representation of mixed layer depth in the Argo float case study. Conversely the KPP model of Large et al. (1994) was found to give a good representation of the mixed layer depth at OWS Papa, provided the vertical resolution was sufficiently high, however when the KPP model was validated using the Argo float the mixed layer depth was found to be too shallow. In both the OWS Papa experiment and the Argo float case study the effect of the net freshwater input from the forcing fluxes was found to have an impact on the modelled mixed layer depth although the effect was not dominant over the annual cycle.

The Kraus–Turner model was tuned using both Argo data and OWS Papa data and the results were found to be consistent, in the absence of data assimilation. In models with no ongoing data assimilation parameter values of $\lambda = 1.0$–$1.1$ and $\delta = 30$–$40$ m are near-optimum in both cases. Results from tuning using Argo data show that if data assimilation is included in the model a larger value of $\lambda = 1.5$ is required but the preferred value of $\delta$ is not altered. Assimilation was found to increase the temperature gradient in the model thermocline such that a larger input of TKE is required to reproduce observed mixed layer deepening. The $\lambda$ parameter, describing the generation of mixing energy, and the $\delta$ parameter, describing the decay of mixing energy, were related by requiring that a fixed amount of mixing energy reach the base of the typical well mixed layer. The resulting simple relation gave a good representation of the interaction between the $\lambda$ and $\delta$ parameters.

## Acknowledgements

The authors thank Paul Martin for providing the met data used in the OWS Papa study and Simon Josey for providing help with the flux parameterisations. The authors also thank Mike Bell, Chris Gordon, Adrian Hines, Matt Martin, Mike McCulloch and David Woolf.

The Argo data were collected and made freely available by the International Argo Project and the national programmes that contribute to it (http://www.argo.ucsd.edu and http://argo.jcommops.org). Argo is a pilot programme of the Global Ocean Observing System.

## References

Bell, M.J., Acreman, D., Barciela, R., Hines, A., Martin, M.J., Sellar, A., Stark, J., Storkey, D., 2004. The forecasting ocean assimilation model (FOAM) system. In: 35th COSPAR Scientific Assembly. p. 1730.

Burchard, H., 2001. Simulating the wave enhanced layer under breaking surface waves with two-equation turbulence models. J. Phys. Oceanogr. 31, 3133.

Burchard, H., Baumert, H., 1995. On the performance of a mixed layer model based on the k-turbulence closure. J. Geophys. Res. 100, 8523–8540.

Burchard, H., Bolding, K., 2001. Comparative analysis of four second-moment turbulence closure models for the oceanic mixed layer. J. Phys. Oceanogr. 31, 1943–1968.

Burchard, H., Bolding, K., Villarreal, M., 1999. GOTM – a general ocean turbulence model. Theory, applications and test cases. Tech. Rep. EUR 18745 EN, European Commission.

Canuto, V.M., Cheng, Y., Dubovikov, M.S., 2001. Ocean turbulence I: one-point closure model. Momentum and heat vertical diffusivities with and without rotation. J. Phys. Oceanogr. 31, 1413–1426.

Craig, P.D., Banner, M.L., 1994. Modeling wave-enhanced turbulence in the ocean surface layer. J. Phys. Oceanogr. 25, 2546.

Davis, R.E., deSzoeke, R., Niiler, P., 1981. Variability in the upper ocean during MILE. Part II modeling the mixed layer response. Deep-Sea Res. 28A (12), 1453–1475.

Dobson, F.W., Smith, S.D., 1988. Bulk models of solar radiation at sea. Q. J. Roy. Meteor. Soc. 114, 165–192.

Fairall, C.W., Bradley, E.F., Hare, J.E., Grachev, A.A., Edson, J.B., 2003. Bulk parameterization of air–sea fluxes: updates and verification for the COARE algorithm. J. Clim. 16, 571–591.

Gaspar, P., 1988. Modeling the seasonal cycle of the upper ocean. J. Phys. Oceanogr. 18, 161–180.

Gaspar, P., Grégoris, Y., Lefevre, J., 1990. A simple eddy kinetic energy model for simulations of the oceanic vertical mixing: tests at Station Papa and long-term upper ocean study site. J. Geophys. Res. 95 (14), 16179–16193.

Gordon, C., Cooper, C., Senior, C., Banks, H., Gregory, J.M., Johns, T.C., Mitchell, J.F.B., Wood, R.A., 2000. The simulation of SST, sea ice extents and ocean heat transports in a version of the Hadley Centre coupled model without flux adjustments. Clim. Dynam. 16, 147–168.

Jerlov, N.G., 1976. Marine Optics. Vol. 14 of Elsevier Oceanography Series. Elsevier.

Johns, T.C., Durman, C.F., Banks, H.T., Roberts, M.J., McLaren, A.J., Ridley, J.K., Senior, C.A., Williams, K.D., Jones, A., Rickard, G.J., Cusack, S., Ingram, W.J., Crucifix, M., Sexton, D.M.H., Joshi, M.M., Dong, B.-W., Spencer, H., Hill, R.S.R., Gregory, J.M., Keen, A.B., Pardaens, A.K., Lowe, J.A., Bodas-Salcedo, A., Stark, S., Searl, Y., 2006. The new Hadley Centre climate model HadGEM1: evaluation of coupled simulations. J. Clim. 19, 1327–1353.

Josey, S.A., Kent, E.C., Taylor, P.K., 1998. The Southampton Oceanography Centre (SOC) ocean-atmosphere heat, momentum and freshwater flux atlas. Tech. Rep. 6, 30pp, plus figs.

Josey, S.A., Pascal, R.W., Taylor, P.K., Yelland, M.J., 2003. A new formula for determining the atmospheric long-wave flux at the ocean surface at mid-high latitudes. J. Geophys. Res. 108 (C4), 3108.

Kantha, L.H., Clayson, C.A., 1994. An improved mixed layer model for geophysical applications. J. Geophys. Res. 99 (18), 25235–25266.

Kara, A.B., Rochford, P.A., Hurlburt, H.E., 2000. An optimal definition for ocean mixed layer depth. J. Geophys. Res. 105 (C7), 16803–16822.

Kraus, E.B., Turner, J., 1967. A one dimensional model of the seasonal thermocline II. The general theory and its consequences. Tellus 19, 98–106.

Large, W.G., 1996. An observational and numerical investigation of the climatological heat and salt balances at OWS Papa. J. Clim. 9 (Aug.), 1856–1876.

Large, W.G., McWilliams, J.C., Doney, S.C., 1994. Oceanic vertical mixing: a review and a model with a nonlocal boundary layer parameterization. Rev. Geophys. 32 (November), 363–403.

Martin, P.J., 1985. Simulation of the mixed layer at OWS November and Papa with several models. J. Geophys. Res. 90 (9), 903–916.

McCulloch, M.E., Alves, J.O.S., Bell, M.J., 2004. Modelling shallow mixed layers in the north-east Atlantic. J. Marine Syst. 52 (December), 107–119.

Mellor, G.L., 2001. One-dimensional, ocean surface layer modelling: a problem and a solution. J. Phys. Oceanogr. 31, 790.

Mellor, G.L., Yamada, T., 1974. A hierarchy of turbulence closure models for planetary boundary layers. J. Atmos. Sci. 31, 1791–1806.

Paulson, C.A., Simpson, J.J., 1977. Irradiance measurements in the upper ocean. J. Phys. Oceanogr. 7, 952–956.

Payne, R.E., 1972. Albedo of the sea surface. J. Atmos. Sci. 29, 959–970.

Pollard, R.T., Millard, R.C., 1970. Comparison between observed and simulated wind-generated inertial oscillations. Deep-Sea Res. 17, 813–821.

Rodi, W., 1987. Examples of calculation methods for flow and mixing in stratified fluids. J. Geophys. Res. 92, 5305–5328.

Simonot, J.-Y., Le Treut, H., 1986. A climatological field of mean optical properties of the world ocean. J. Geophys. Res. 91 (C5), 6642–6646.

Smith, S.D., Dobson, F.W., 1984. The heat budget at Ocean Weather Station Bravo. Atmos. Ocean 22, 1–22.

Stips, A., Burchard, H., Bolding, K., Eifler, W., 2002. Modelling of convective turbulence with a two-equation k-$\epsilon$ turbulence closure scheme. Ocean Dynam. 52, 153–168.

Thomson, R., 1976. Climatological numerical models of the surface mixed layer of the ocean. J. Phys. Oceanogr. 6, 496–503.